Applied Nanoscience
https://doi.org/10.1007/s13204-021-01687-w

ORIGINAL ARTICLE

Antimicrobial composites of nanoparticles generated by gamma irradiation supported in clinoptilolite-rich tuff

C. Martínez-Vieyra[1,2] · E. Gutiérrez-Segura[3] · G. López-Tellez[4] · D. Alcántara-Díaz[2] · M. T. Olguín[2]

Received: 13 November 2020 / Accepted: 19 January 2021
© King Abdulaziz City for Science and Technology 2021

Abstract

In developing countries, rates of hydric illness in children are high because of the consumption of non-potable water. Therefore, it is important to investigate new methodologies to diminish microorganisms' concentration in the water that is used in rural areas for drinking. Microbicide agents with a base of natural zeolites can be an alternative to water disinfection instead of using other kinds of disinfectants that produce by-products. Hence, the synthesis and characterization of metallic or oxide-metallic nanoparticles-natural zeolite composites to evaluate the antimicrobial activity in front of *Salmonella typhimurium* and *Candida albicans* in this work were investigated. The natural zeolite was in contact with salt solutions of Ag, Cu, or Zn to obtain the modified natural zeolites, and they were then gamma irradiated to generate the nanoparticles. The samples were characterized by different techniques. The *Salmonella typhimurium* and *Candida albicans* were suspended in distilled water and put in contact with the composites at different times. The kinetic of the cellular decay was obtained using the Chick model. The chemical species of the nanoparticles obtained were Ag, Cu_2O, and ZnO. The kinetic parameter of the cell decay of both *Salmonella typhimurium* and *Candida albicans* is the biggest for silver nanoparticles-natural zeolite composite (Z-NpsAgγ). Between two independent experiments of the cellular decay, differences in the *k* values were observed. The antimicrobial activity of these composites depends on the characteristics of each microorganism, the mass of the composite, the content of the metallic or oxido-metallic nanoparticles in the natural zeolites, their distribution on the zeolitic material surfaces, and the chemical species obtained during the gamma irradiation. The Z-NpsAgγ could be an alternative for water potabilization.

Keywords Metallic and oxide metallic nanoparticles · Microorganism · Microbial mortality · Natural zeolites

Introduction

Biological water contamination is a global problem; however, it is accentuated in developing countries, where the most vulnerable populations (like poor kids) continuously get sick and even die from enteric infections (Batistela et al. 2017; Bertrand et al. 2015). Several factors contribute to this situation, such as the amount of fecal waste generated by growing populations and animal production, wastewater disposal without any treatment, which pollutes the increasingly scarce sources of drinking water, and the increasing use of antibiotics and effluents of pharmaceuticals, which have enhanced the resistance of several strains of bacteria. Amini and Kraatz (2014), as well as Ashbolt (2015), reported a list of microbial pathogens present in drinking water and that represented a risk of gastrointestinal diseases; among these are recognized viruses (such as Rotavirus, Hepatitis A and E), bacteria (*Salmonella enterica*, *Shigella*

✉ M. T. Olguín
teresa.olguin@inin.gob.mx; olguingmt@gmail.com

1 Doctorado en Ciencia de Materiales, Facultad de Química, Universidad Autónoma del Estado de México, Paseo Colón y Tollocan S/N, C.P. 50000 Toluca, Estado de México, Mexico

2 Instituto Nacional de Investigaciones Nucleares, Carretera México-Toluca S/N La Marquesa, C. P. 52750 Ocoyoacac, Mexico

3 Facultad de Química, Universidad Autónoma del Estado de México, Paseo Colón y Tollocan S/N, C.P. 50000 Toluca, Estado de México, Mexico

4 Centro Conjunto de Investigación en Química Sustentable, Universidad Autónoma del Estado de México, Universidad Nacional Autónoma de México, Carretera Toluca-Ixtlahuaca Km. 14.5, Tlachaloya, Toluca, Mexico

Published online: 05 February 2021

sonnei, *Vibrio cholerae*, *Campylobacter jejuni*), and protozoan (*Cryptosporidium hominids*, *Giardia intestinalis*, *Toxoplasma gondi*).

Salmonella typhimurium, which belongs to the prokaryote cell group, is a pathogen bacterium. It causes gastroenteritis and colitis (Shuai-Cheng et al. 2016), is widely distributed in several environments and can contaminate water and foods (Koopman et al. 2015). It is characterized by the formation of biofilm aggregations when they colonize intestinal epithelium or in solid surfaces, which makes it persistent. *Candida albicans* is a microorganism that can grow both as yeast and as filamentous fungi. It is a part of the organisms that make up the human flora. However, it is an opportunistic pathogen that can cause infection in immunosuppressed patients (Sellam and Whiteway 2016). It can form biofilms, too (Olorode and Okpokwasli 2012).

A wide diversity of microorganisms exists inside our environment. Most benefit because they are part of normal human flora, for the role they play in the trophic chain, or for their use in various processes linked to human economic activities, such as fermentation. However, there is another, which is harmful to human, vegetal, and animal health. Therefore, several antimicrobial agents, such as heat (with inherent energy consumption) and halogenated compounds, especially chlorine and its derivatives, have been used to prevent the contamination of this pathogen in water. However, these can form toxic by-products, like colloidal and ionic silver, to name a few. Currently, the possibility of using filters of various materials, like polymers or zeolites supporting nanoparticles of metal or metal oxides, is opened, due to the combination of nanoparticles (NPs) reactivity with the high surface area and slow-release rate of zeolites, such as clinoptilolite (Copcia et al. 2011).

Inside the group of nanoparticles, which are used for antimicrobial purposes, metallic silver, copper, and zinc oxides stand out as they cause damage to the cell wall, penetrating and piling up at the membrane and interfering with the metabolic activities of bacteria and yeast. Further, these NPs produce oxidative stress, damaging lipids, proteins, carbohydrates, and nucleic acids (Siddiqi et al. 2018).

Zeolites are crystalline-hydrated aluminosilicates materials which have basic tetrahedral units. The central position can be occupied by silica or aluminum. atoms (Abidin et al. 2017). The tetrahedral corner has oxygen atoms, which are shared with other tetrahedral units to form a framework structure with cavities, cages, and channels, giving place to three-dimensional structures. The presence of the aluminum atom instead of silica generates a negative charge onto one oxygen atom that can be balanced by several ions such as sodium, potassium, calcium, and magnesium (named extra framework cations), which can be exchanged by other ones. This fact is very important as it generates the capacity of the ion exchange, one of the most important properties of the zeolites, as reported by Dong et al. (2017). Another banner characteristic in these materials is the presence of water molecules located inside the zeolite structure, which can be removed with the final purpose of generating a place that can be taken for similar species regarding size, shape, and polarity, as mentioned by Li and Yu (2014). Added to this, Li et al. (2017) describe that the zeolites can form composite materials because they possess a big surface area and can support metal nanoparticles or metal clusters to help them with adequate distribution and stabilization.

Several composites with clinoptilolite supporting metal and metal oxide nanoparticles have been used as a microbicide or bacteriostatic agent (Shaw et al. 2016) against different pathogen microorganisms (Lingaraju et al. 2016). Clinoptilolite is a natural zeolite, which, by its structural characteristics, belongs to the heulandite group (Alver et al. 2010). Concerning the clinoptilolite crystal structure, it possesses a unit cell monoclinic C centered. The chemical elements of clinoptilolite are Al_7 Si_{29} with 72 oxygen atoms, 24 H_2O molecules, and cations as Na, K, Ca, and Mg (Sareban and Javanbakht 2017). This mineral is abundant in several deposits of the world (Ambrozova et al. 2017), additionally, it is easily obtained from them. It allows for these materials to be used in hybrid nanostructures, as reported by Yu et al. (2019). In particular, a combination of clinoptilolite and metal or metal oxide nanoparticles leads to composites with potential applications (Khodadadi et al. 2017; Bordbar et al. 2017) besides that the supports facilitate to separate the NPs at the end of the process (Batistela et al. 2017).

Gamma radiation is a method for metallic nanoparticle synthesis that has the advantage of being able to be used with several supports, such as zeolites (Clifford et al. 2017); this will not affect their crystalline structure. Gamma rays are electromagnetic radiations with high energy. When these hit an aqueous suspension of exchanged metallic zeolites, they disrupt water molecules, generating various chemical species; the solvated electrons and hydrogen radicals are most important for the reduction process. However, in the reaction media are also (•OH) hydroxyl radicals, which are strong oxidizers. For a reduction media, isopropyl alcohol is used as hydroxyl radicals scavenger because the radical (•OH) takes out an electron from alcohol, giving place to isopropyl radical, a more stable species, which turns into reductor agent, too. After, the atoms of metallic species coalesce to form nucleation centers and posteriorly grew up in nanoparticles and clusters (Sheikh et al. 2009). Moreover, the dose ratio is a powerful tool to control the NPs. Belloni reported in 2006 that when a high dose rate is employed, all reduced species are rapidly formed, then they coalesced and form the nucleus, while with a low dose rate, the nucleation of reduced metal atoms is faster than the rate production, meaning that reduction of metal atoms occurred over those already formed, leading to larger sizes. Outstanding qualities

of this method include the fact that it reduces the possibility of chemical poisoning of the nanocomposites obtained, avoids the use of stronger chemical reductors such as hydrazine hydrate (Du et al. 2017), can control the shape and size of metallic nanoparticles varying doses parameters and stabilized agent (Flores-Rojas et al. 2018), and the products can easily purify.

Therefore, this paper aimed to synthesize and to characterize composites of clinoptilolite supporting nanoparticles of Cu, Ag, and Zn using gamma rays from ^{60}Co source to promote them, as well as to describe the antimicrobial behavior of these composites for the water disinfection considering the kinetics of the processes, using *Salmonella typhimurium* and *Candida albicans* for their structural differences. Furthermore, both are found in polluted water.

Methods

Reagents and equipment

The natural zeolite used in this work was recollected from deposits located in Etla, Oaxaca, México. The principal mineral phases of this zeolitic material are clinoptilolite, mordenite, quartz, and feldspar, as will be discussed later. Silver nitrate ($AgNO_3$) and sodium chloride (NaCl) were procured from Merck Chemicals. Copper nitrate hemipentahydrate ($Cu(NO_3)_2{\cdot}2.5H_2O$) and zinc nitrate hexahydrate ($Zn(NO_3)_2{\cdot}6H_2O$) were obtained from Sigma-Aldrich Chemicals. Isopropanol was supplied from Tecsiquim S.A. de C.V.

The morphology of the clinoptilolite supporting the metal nanoparticles was obtained employing Scanning Electron Microscopy (SEM) using a JEOL model JSM-5900LV coupled to the DX-4 probe to obtain the elemental composition by X-ray Energy Dispersive Spectroscopy (EDS); fixed with the field of SEM. Test of three different areas of the material was accomplished for natural zeolite in its sodic form (Z-Na) and every composite at 500X, getting the average % wt. The shape and size of nanoparticles (NPs) were observed and captured with a transmission electron microscopy (TEM) JEOL model JEM-2010, which operates at 120 kV accelerating voltage, equipped with a camera, model ORCAFLASH40CHAM; subsequently, the NPs diameters were measured using Image J program. Sample preparation was done suspending crush composites (using an Agatha mortar) in ethanol and sonicating them for 5 min; a drop of this suspension was placed on a grid of carbon-coated copper. In the case of Cu nanoparticles-natural zeolite composite (Z-NPsCuγ), a carbon-coated nickel grid was used, so avoid the copper's grid interference. A D8 Discover diffractometer was used to record the X-ray diffraction patterns (XRD) of the samples with Cuα radiation ($\lambda = 1.5406$ Å). The scanning was done in the region of 4°–60° 2θ. X-ray photoelectron spectroscopy (XPS) was employed to investigate the composition of every composite as well as the chemical states of metal NPs using a Thermo Scientific model K-Alpha with an Al Kα line (1486.5 eV). For the measurement of the BET surface area and pore-size diameter of composites, a nitrogen adsorption–desorption analyzer model BELSORP-28SA was used. The amount of Ag, Cu, and Zn of NPs supported in the composites after gamma irradiation was known to employ neutron activation analysis (NAA), using the nuclear reactor TRIGA MARK III, in the rotatory system capsule for 30 min or 2 h depending on the metal to be quantified, at the same time of reference patterns, then the specific radioactivity was determined using High-purity Germanium detector.

Zeolite conditioning

Clinoptilolite was crushed and sieved to obtain fractions with a size between 0.5 and 0.7 mm (designated as Z-N). Afterward, a mixture of 200 g of the zeolitic material and 500 mL of 0.1 M NaCl solution was refluxed for 24 h. The sodium zeolite resultant was rinsed with distilled water repeatedly until chloride elimination was verified by the $AgNO_3$ test. Finally, it was dried at 75 °C for 5 h, and the sample was designated as Z-Na.

Exchanged zeolites

Samples of 50 g of Z-Na were placed in a flat bottom ball flask, and 200 mL of 0.1 M of $AgNO_3$; $Cu(NO_3)_2{\cdot}2.5H_2O$ or $Zn(NO_3)_2{\cdot}6H_2O$ solutions were added; next, the reactions mixture was refluxed for 12 h (twice). Later, the exchanged zeolites that resulted were filtered using a filter paper, washed with distilled water, and dried at 75 °C for 5 h. These samples were named Z-Ag, Z-Cu, and Z-Zn.

Gamma radiation to nanocomposites synthesis

In 20-mL flasks, 5 g of each exchange zeolite (Z-Ag, Z-Cu, and Z-Zn) was suspended in 10 mL of isopropanol, and then, the flasks were covered with a septum and brought to bubbling with high-purity nitrogen for 10 min. Then, the samples were sealed and irradiated, at ambient conditions, with a ^{60}Co γ-ray source at a dose rate of 0.756 kGy/h and a total dose of 40 kGy. Then, individually, the samples were filtered and washed twice; finally, they were dried at 75 °C for 5 h. The different composites obtained were named Z-AgNPsγ, Z-CuNPsγ, and Z-ZnNPsγ.

Disinfection

Indicators of biological contamination

The gram-negative bacterium *Salmonella typhimurium* (*S. typhimurium*) ATCC14028 and the yeast *Candida albicans*

(*C. albicans*) ATCC10231 were chosen as representative microorganisms of biological water contamination.

Overnight culture

The microorganisms *S. typhimurium* and *C. albicans* were cultured in tryptic soy broth (TSB) and liquid Luria Bertani (LB) respectively, at 37 °C for 19 h, using a gyratory water bath shaker; then, the cells were centrifuged at 10,000 rpm at 4 °C (to stop the microbial growth), washed and, finally, suspended in distilled water, obtaining a final concentration of 1×10^9 CFU/mL for the bacteria and 5×10^8 CFU/mL for the yeast. Subsequently, decimal dilutions were made to achieve optimal colony growth when in a Petri dish. It is important to mention that CFU/mL stands for colony-forming unit of bacteria or yeast per milliliter, and in this work, it was used to assess the number of viable cells in an aqueous solution at different times to obtain the decay kinetics for the microorganism.

Antimicrobial effect

With the purpose of determining the antimicrobial effect of the zeolites Z-CuNPsγ, Z-AgNPsγ, and Z-ZnNPsγ on *S. typhimurium* and *C. albicans*, two microbial suspensions were prepared separately, consisting of 100 mL of distilled and sterilized water and 1 mL of cells (from an overnight culture dilution) of each microorganism and adding 10 mg of Z-AgNPsγ, 200 mg of Z-CuNPsγ and Z-ZnNPsγ, in the case of *S. typhimurium* and 200 mg of Z-AgNPsγ or 2000 mg of Z-CuNPsγ and Z-ZnNPsγ for *C. albicans.* The mixtures were under constant stirring, and keeping at 37 °C, the corresponding aliquots (0.1 ml) were taken for triplicate at 0, 7.5, 15, 30, 60, 120, 180, 240, 300, 360, 420 min, or until the 100% microbial mortality was achieved. Two independent experiments for each system (Z-NPs-microorganisms) were carried out. These were named experiment 1 and experiment 2.

The amounts of each composite (Z-AgNPsγ, Z-CuNPsγ, and Z-ZnNPsγ) were chosen based on preliminary experimentation to find the best conditions to describe the kinetic behavior of the cellular decay.

Microorganism quantification

The aliquot was taken for every time (for triplicate), were filtered using a micropore cellulose-nitrate membrane (diameter of 0.45 µM, Millipore), and then put in bismuth sulfite agar or Luria Bertani culture media for the quantification of *Salmonella typhimurium* and *Candida albicans,* respectively. Later incubation, the CFU (colony forming units) in the Petri dishes were quantified.

Chick model

Chick's law represents the inactivation of microorganisms, which follows a kinetic of first order considering that the antimicrobial agent concentration is constant.

The linearized form of this model is represented as:

$$\mathrm{Ln}\left(\frac{N_t}{N_o}\right) = -kt$$

where N_t = concentration of microorganisms at time t (CFU/mL), N_o = initial concentration of microorganisms (CFU/mL), k = kinetic constant that shows the cellular decay velocity (min^{-1}), t = time (min).

This model has been used to describe the kinetic process of water disinfection using different microbicides (Ganguly et al. 2018; Ateia et al. 2020).

Results and discussion

Morphology

SEM allows obtaining information about zeolite morphology besides the identification of characteristics phases, which composed the material, and it can be confirmed using XRD (Polychroniadis et al. 2013). Figure S1a shows the image of Z-Na, obtained after conditioning of natural zeolite with NaCl solution to improve the capacity of ion exchange of zeolitic material, the classical monoclinic symmetry of the clinoptilolite was observed, which is similar to that reported by Favvas et al. (2016), and it is the main component of the material, but some fibers corresponding to orthorhombic symmetry of mordenite is also observed (Mansouri et al. 2013). In the figures S1b–S1d of the exchanges zeolites, Z-Cu, Z-Ag, and Z-Zn respectively, it can be observed that the crystalline structure is preserved after the exchange treatment with the corresponding salts ($AgNO_3$, $Cu(NO_3)_2 \cdot 2.5H_2O$ and $Zn(NO_3)_2 \cdot 6H_2O$) (De la Rosa-Gómez et al. 2008).

Figure 1 shows the composites obtained after gamma irradiation (Z-AgNPsγ, Z-CuNPsγ, and Z-ZnNPsγ), and it can be seen that the crystalline structure of the natural zeolite is conserved in all the cases, which is one of the important aspects of employing this method to obtain the nanoparticles supported on it. In the case of silver, contrasting points can be observed where silver clusters are located, generated by gamma irradiation (Singh et al. 2015). However, Panayotova et al. (2018) found that the zeolite changed its morphology after the modification with the silver under their experimental conditions (0.1 M of $AgNO_3$ solution in contact with the natural zeolite during 2 h and treated at 400 °C).

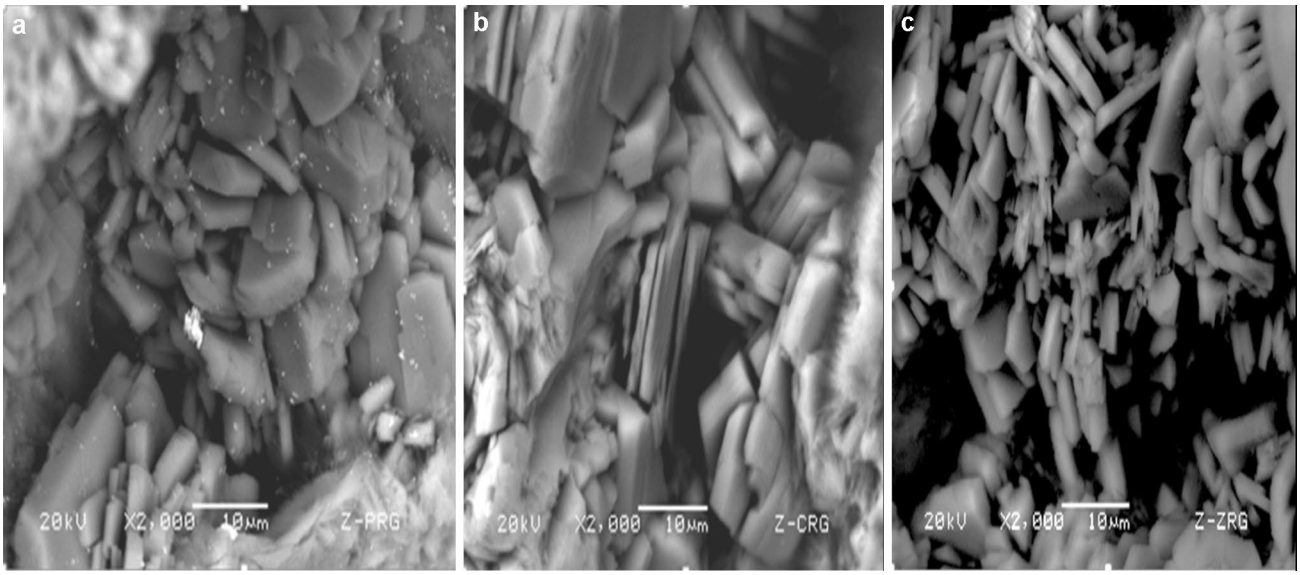

Fig. 1 SEM images of Z-AgNPsγ (**a**), Z-CuNPsγ (**b**), Z-ZnNPsγ (**c**)

Elemental composition

Results depicted in Table 1 confirm the presence of several elements in the Z-Na, Z-Ag, Z-Cu, and Z-Zn such as oxygen, silica, and aluminum, which are the primary constituents of aluminosilicates (Alswat et al. 2017), besides the extra reticular cations like Na^+, K^+, Ca^{2+}, and Mg^{2+}. The Na^+ and K^+ were involved in the ion exchange processes to obtain the modified natural zeolites. The Na (wt%) diminished 2.6, 3.6, and 1.8 times after the contact with the Ag^+, Cu^{2+}, and Zn^{2+} nitrate solutions, respectively. However, the K^+ slightly decreased (1.2 times) for the case of the Z-Ag. The contents (in wt%) of Ag, Cu, and Zn in the Z-Ag, Z-Cu, and Z-Zn were 10.7 ± 1.6, 3.3 ± 0.2 wt.%, and 1.3 ± 0.3 wt.%. After the gamma irradiation of these materials, the amount of the metallic species does not notably change, except for Z-Zn and Z-NPsZn. This result could be due to the semi-quantitative character of the EDS technique or because of the heterogeneity distribution of the Zn on the surface of the natural zeolite.

Nanoparticle size distribution

Figure 2 shows the TEM images and size histograms of the nanoparticles supported in zeolites obtained after gamma irradiation; the first one is for silver composite (Z-AgNPsγ) (Fig. 2a), in which observed nanoparticles with semi-spherical shape and mean size of 4.6 nm (± 1.41); the second one is for copper composite (Z-CuNPsγ) (Fig. 2b) with a spherical shape and a mean diameter of 4.0 nm (± 1.0); finally, the composite of Zn (Z-ZnNPsγ) (Fig. 2c), has a spherical shape and mean diameter of 5.0 nm (± 1.4). Uniformly generated

Table 1 Elemental composition of exchanged zeolites and composites

Element	Z-Na Weight %	Z-Ag	Z-NpsAgγ	Z-Cu	Z-NPsCuγ	Z-Zn	Z-NPsZnγ
O	46.0 ± 0.9	45.6 ± 0.6	44.2 ± 1.5	46.0 ± 1.2	43.0 ± 1.9	41.8 ± 4.7	43.59 ± 2.86
Na	2.9 ± 0.1	1.1 ± 0.1	1.0 ± 0.2	0.5 ± 0.3	0.8 ± 0.1	1.4 ± 0.1	1.67 ± 0.21
Mg	0.1 ± 0.1	0.1 ± 0.1	0.1 ± 0.1	0.2 ± 0.1	0.1 ± 0.1	0.1 ± 0.1	0.12 ± 0.08
Al	6.9 ± 0.1	6.4 ± 0.4	6.4 ± 0.4	7.1 ± 0.1	7.1 ± 0.4	6.9 ± 0.3	7.19 ± 0.37
Si	40.7 ± 0.5	34.2 ± 1.0	35.6 ± 1.0	38.0 ± 1.1	40.5 ± 0.6	38.1 ± 1.1	40.53 ± 1.15
K	2.2 ± 0.5	1.3 ± 1.0	1.8 ± 0.3	3.2 ± 1.0	2.6 ± 0.8	2.2 ± 0.6	2.14 ± 0.80
Ca	0.7 ± 0.1	0.5 ± 0.1	0.5 ± 0.1	0.5 ± 0.1	0.6 ± 0.1	0.6 ± 0.2	0.64 ± 0.14
Ag	ND	10.7 ± 1.6	11.3 ± 1.7	ND	ND	ND	ND
Cu	ND	ND	ND	3.3 ± 0.2	4.6 ± 0.3	ND	ND
Zn	ND	ND	ND	ND	ND	1.3 ± 0.3	4.1 ± 0.7

ND no detected

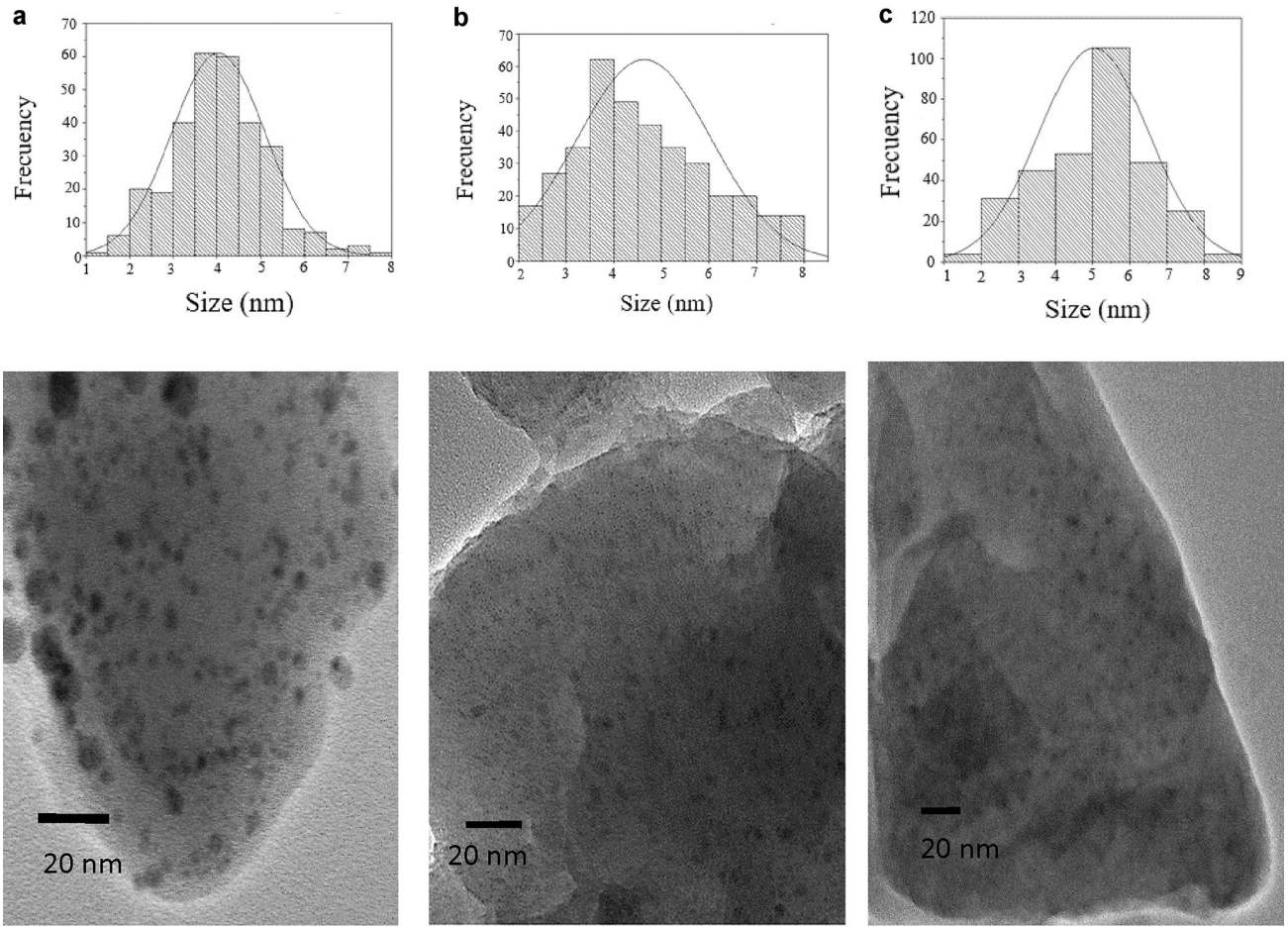

Fig. 2 TEM image and histogram of the distribution of particle size of Z-AgNPsγ (**a**), Z-CuNPsγ (**b**) and Z-ZnNPsγ (**c**)

in situ reduction agents (solvated electrons and hydrogen radicals) are an advantage of this method; therefore, similar sizes are created at a specific dose of gamma irradiation (Shameli et al. 2010), which in the case of present work was 40 kGy. Furthermore, the metallic ions are supported on the zeolite surface first, and then, they are reduced there. Therefore the dispersion of these is limited and results in small metallic clusters (Belloni et al. 2018). It important the fact that all shapes of the NPs obtained are spherical. Cheon et al. (2019) emphasized the relation between morphology and antimicrobial activity due to the surface area of nanoparticles.

Mineral composition and crystallinity

The XRD patterns of the different zeolitic materials are shown in Fig. S2, and they include the exchange zeolites Z-Ag (Fig. S2a), Z-Cu (Fig. S2b), and Z-Zn (Fig. S2c), located at the left column and the metallic or oxide-metallic nanoparticles-natural zeolite composites obtained after gamma irradiation: Z-AgNPsγ (Fig. S2d), Z-CuNPsγ (Fig. 4e) and Z-ZnNPsγ (Fig. 4f), given at the right column.

In all the patterns showed in the same Fig. S2 can be noted that the zeolite crystalline framework is conserved. However, strong zeolite peaks overshadow the peaks of metallic nanoparticles (Boruban and Nalbant Esenturk 2017). The natural zeolite exhibits reflexions at 2θ = 9.89, 22.25, 27, 30.85, which correspond to clinoptilolite according to card JCPDS 39-1383, similar to those reported by Ullah et al. (2019). This zeolitic material also presents reflexions at 2θ = 6.46, 19.58, 25.67 to card PDF00-060-0846 from mordenite mineral (Hussain and Mohammed 2019) and small amounts of quartz, as well as feldspar (46-1045 and 83-1370 JCPDS cards, respectively). Pérez-González et al. (2020) found similar components in the natural zeolite from Tlacolula de Matamoros from Oaxaca (Mexico). However, in that case, the natural zeolite was richer in mordenite than in clinoptilolite.

The apparent differences in the number of reflexions found in the X-ray diffraction patterns of Z-Ag (Fig. S2a) and Z-NPsAgγ (Fig. S2d) could be due to the high intensity

of the reflexion observed at 27 2θ (Fig. S2a), which does not permit the definition of the other reflexions with less intensity. These results could be due to incorporating the Ag in the ion exchange sites of the zeolite network. When this silver exchanged zeolite (Z-Ag) is irradiated using a ^{60}Co source, the formation of nanoparticles is carried, and the signals are well defined (Fig. S2d). It is also important to consider that the Ag is present in the zeolitic material in a greater quantity than Cu or Zn. For this reason, no notable changes were appreciated in the corresponding X-ray diffraction patterns (Figures S2b, S2c, S2e, and S2f).

The nanoparticles of Ag (Lanje et al. 2010) present reflexions at 34.5 and 46.9 2θ (JCPDS 04-0783), corresponding to Cu_2O (Feng et al. 2012) at 36 and 43 2θ (JCPDS 05-0667) and finally the nanoparticles of ZnO (Bouzourâa et al. 2016) at 31.8, 34.5, and 36.2 2θ (JCPDS 36-1451). However, only the reflexions of the Ag nanoparticles from the composite were observed.

Chemical speciation

Figure S3 shows the core level spectrum of the composites of silver, copper, and zinc, respectively. Z-AgNPsγ (Fig. S3a) has two peaks: Ag 3d5/2 with binding energy at 369.5 eV, and Ag 3d3/2 at 375.6 eV. The energy gap between the characteristic silver signals is 6.1 eV, which corresponds to metallic silver, as reported by Sharma et al. (2018). Z-CuNPsγ (Fig. S3b) shows two main signals at 934.2 and 954.0 eV, which can be assigned at Cu (I) 2p3/2 and Cu (I) 2p1/2 orbitals, respectively. Also, the separation between these binding energy signals is 19.8 eV. Shake-up signals can also be observed, which are characteristics of Cu_2O (Biesinger 2017). Finally**,** the XPS spectrum of Z-ZnNPsγ, (Fig. S3c) presents two typical peaks, Zn 2p3/2 at 1024.1 eV and Zn 2p1/2 at 1047.3 eV, which have a separation of 23.2 eV. Both parameters denote the presence of ZnO with Zn (II) (Yu et al. 2019).

There are shifts of the signals toward higher values of binding energy in the three samples: The signal of Ag (0) is displaced with 1.0 eV, the signal of Cu (I) with 1.9 eV (Boruban and Nalbant Esenturk 2017), and the signal of Zn (II) with 2.5 eV (Salama and Ali 2016; Zahmakıran et al. 2011), due to the effect of the clinoptilolite matrix on the oxide metal and metallic NPs (Zahmakiran et al. 2010). It means that the negative charge over the oxygen atoms, generated by aluminum that replaces silica in the zeolite network, attracts to the metallic or oxide-metallic NPs, which have a positive charge density.

Textural parameters

The surface area, total pore volume, and pore diameter of the zeolitic materials are shown in Table S1. The Z-N presents a specific surface area of 8.7 m^2/g, which is small compared to other clinoptilolite-rich tuffs from some regions around the world. Specific surface areas of 84.45 m^2/g for clinoptilolite rock from Aftar have been reported in the literature (Mansouri et al. 2013). However, the clinoptilolite-rich tuff from Sokyrnytsa (Ukrainian Transcarpathian) shows a specific surface area of 14 m^2/g (Korkuna et al. 2006). These contrasting values could be due to the associated mineral components of the zeolitic rock of each geographical area.

The surface area of Z-Na did not change noticeably with respect to Z-N. The surface area increased 1.2 times for Z-CuNPsγ and Z-AgNPsγ, and 1.4 times for Z-ZnNPsγ. These results can be explained by the size of the nanoparticles (Ag, Cu_2O, or ZnO) present on the surface of the modified materials, which did not block the pores of the natural zeolite (León et al. 2016; Abidin et al. 2017; Mahmoodi-Meimand et al. 2020). Other authors observed an increment of the specific surface area of the clinoptilolite when it was summited to different treatments (Moradi et al. 2018; Rodríguez-Méndez et al. 2017).

In the case of the total pore volume and pore diameter of the natural zeolites (Table S1) with metallic nanoparticles supported on them (composites) slightly diminished with respect to Z-Na, probably due to the sites, which the nanoparticles occupy in the channels of the zeolite network. Therefore, the nanoparticles could be occluded in the cavities of the zeolitic materials (Liu et al. 2015; Jafari et al. 2020).

The gamma irradiation of the metallic or oxide–metallic–natural zeolite could contribute to modifying the textural characteristics of the different composites. Gamma irradiation may affect in a similar way than the acid treatment of the natural zeolite, breaking some large pores to generate smaller ones. For this reason, the diameter of the pores of the composite could be diminished (Vergara-Figueroa et al. 2019).

Concentration of the metallic species in the bulk of the composites

NAA is quantitative and representative of the amount of metallic species in the bulk of the composites, not just the surface of these materials (L'Annunziata 2007). In Table 2 are shown the (n,γ) nuclear reactions as well as the results in weight percent of the elements present in the composites. It is outstanding that silver has the highest percentage, followed by copper and zinc as the lowest. Results are important because there is a direct relationship between the amount of the metallic species in the composite and antimicrobial activity.

The sodium content in the materials increases according to the metal that was exchanged to obtain the modified natural zeolites and then the composites when they were

Table 2 Amount of metallic species in the bulk of the composites

Material	Sodium $^{23}Na(n,\gamma)^{24}Na$ Weight (%)	Silver $^{109}Ag(n,\gamma)^{110m}Ag$	Copper $^{63}Cu(n,\gamma)^{64}Cu$	Zinc $^{64}Zn(n,\gamma)^{65}Zn$
Z-NPsAgγ	1.330 ± 0.001	7.160 ± 0.001	ND	ND
Z-NPsCuγ	1.550 ± 0.002	ND	1.910 ± 0.005	ND
Z-NPsZnγ	1.780 ± 0.002	ND	ND	1.200 ± 0.004

ND no detected

exposed to gamma radiation from ^{60}Co. These results could be explained with the base in the ionic radii of each metallic cation, their valence numbers, and the size of the hydrated ions.

Antimicrobial activity

Cellular decay

Figure 3 shows the survival of *S. typhimurium* as a function of contact time with the different composites and the Z-Na for comparison purposes. Z-Na (Fig. 3a), for both series with 10 and 200 mg, corresponding to experiment 1 and 2, respectively, does not present changes regarding bacterial

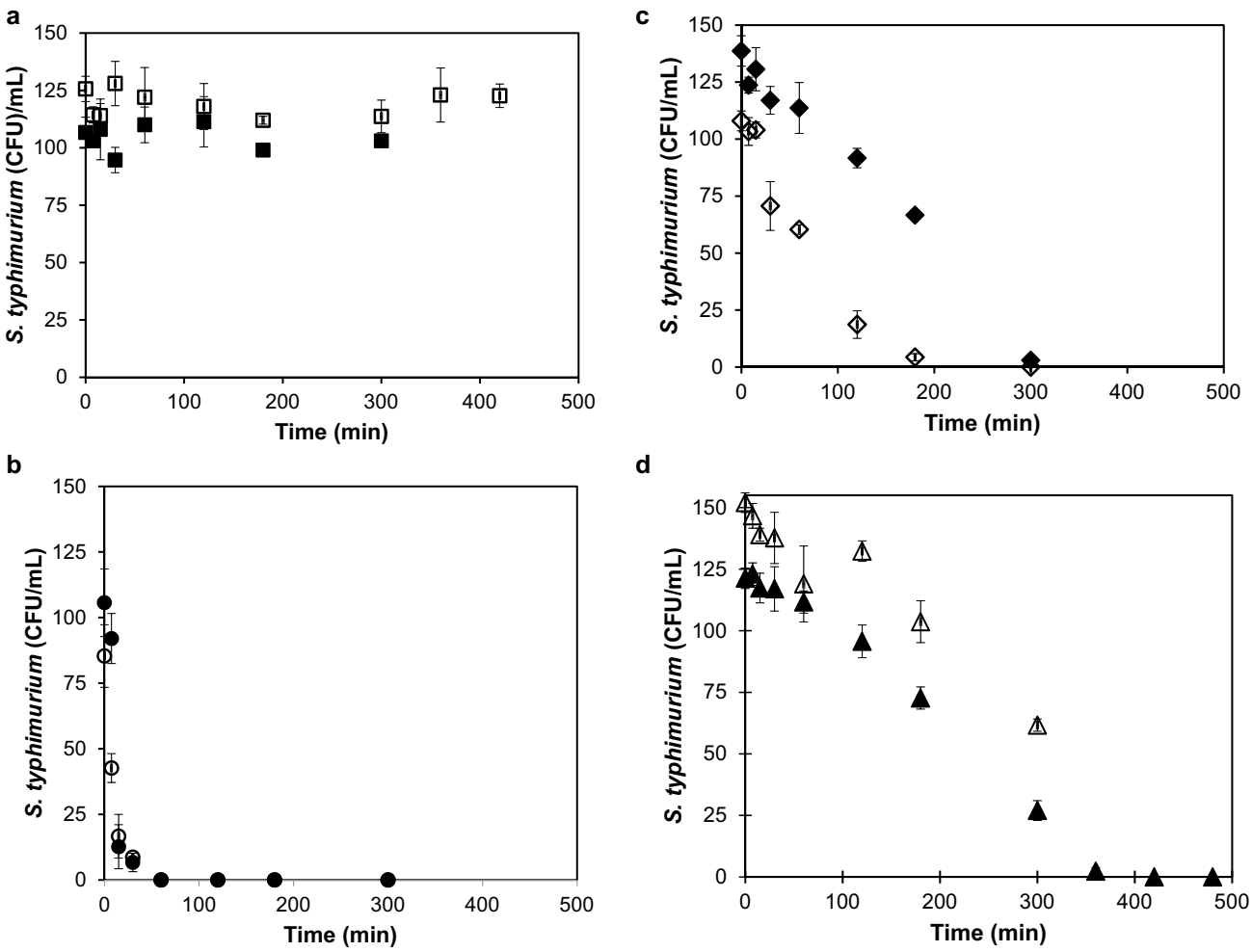

Fig. 3 Survival of *S. typhimurium* against time by ZNa (**a**), ZNPsAgγ (**b**), ZNPsCuγ (**c**), ZNPsZnγ (**d**) for independent experiment 1 (*unfilled symbol*) and experiment 2 (*filled symbol*)

Table 3 Kinetic constants of cell decay (k) of *S. typhimurium* by Z-Na, Z-NPsAgγ, Z-NPsCuγ and Z-NPsZnγ

Sample	Metal content in the bulk of the composites	Mass of composite (mg)	Experiment number (E)	Total inhibition time (min)	k (min^{-1})	R^2	k variation between experiments
Z-Na	2.940 ± 0.150*	10	1	Not observed	NA	NA	NA
		200	2	Not observed	NA	NA	NA
ZNPsAgγ	7.160 ± 0.001	10	1	60	0.0980	0.8612	k_{E1}/k_{E2} 1.2
			2	60	0.0832	0.9356	
ZNPsCuγ	1.910 ± 0.005	200	1	180	0.0095	0.7765	k_{E2}/k_{E1} 1.7
			2	300	0.0162	0.9622	
ZNPsZnγ	1.200 ± 0.004	200	1	Not was reached at 300	0.0027	0.8968	k_{E2}/k_{E1} 2.7
			2	360	0.0074	0.7493	

NA not applied

*Value determined by EDS

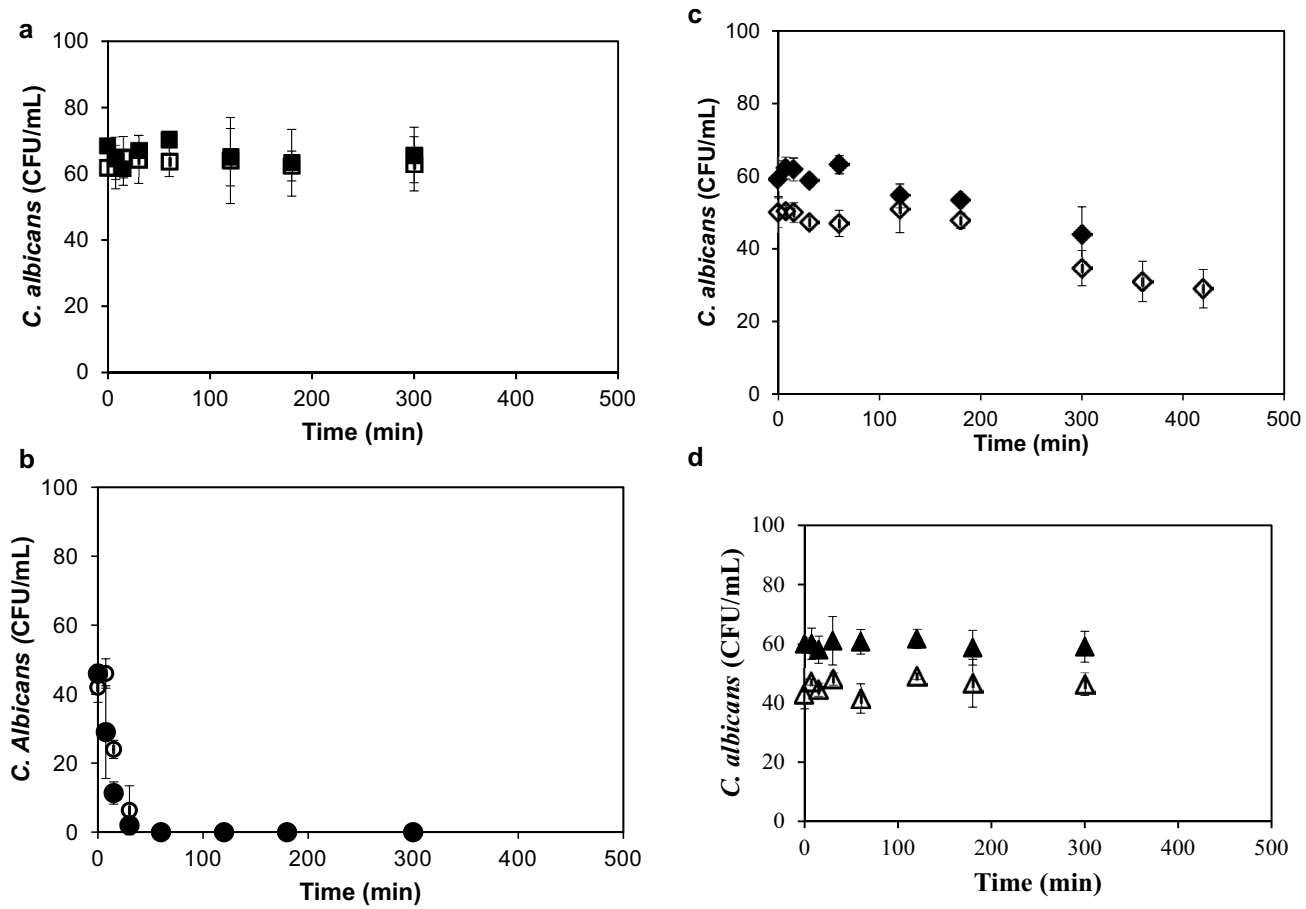

Fig. 4 Survival of *C. albicans* against the time of Z-Na (**a**), Z-NPsAgγ (**b**), Z-NPsCuγ (**c**), Z-NPsZnγ for independent experiment 1 (*unfilled symbol*) and experiment 2 (*filled symbol*)

growth inhibition, due to the fact that sodium has no antimicrobial activity, which agrees with Jiao (2016), who used a zeolite NaY. In the case of Z-NPsAgγ (Fig. 3b) using 10 mg (experiments 1 and 2), in 60 min, 100% of bacterial mortality was achieved, while for Z-NPsCuγ (Fig. 3c), 100% of bacterial mortality was reached but at 180 and 300 min, with 200 mg (experiment 1 and 2, respectively). These differences between the two experiments can be explained by

the heterogeneity of the copper composite obtained. Finally, Z-NPsZnγ (Fig. 3d) is the composite that presents lower bacterial activity, due to at 360 min, 100% of mortality was attained with a mass of 200 mg. As can be observed, the type of metallic species on the zeolitic network, the percentage in the composite, and the mass of these microbicides play a role during the disinfection process (Table 3). However, the characteristics of the *S. typhimurium* could also be playing a role in this process.

ZNPsAgγ is the most efficient since with less mass quantity, in 60 min it eliminates the bacterial growth. A similar result was obtained by Dong et al. (2017). These authors reported the excellent bactericidal efficiency of silver NPs confined in the zeolite EMT. Besides, some authors mentioned that cooper and zinc oxides have antibacterial activity (Alswat et al. 2017; Dizaj et al. 2014); however, it is important to consider that copper and zinc NPs are oxides and silver NPs as Ag^{o} which could affect the interactions with the structure of the microorganism (*S. typhimurium*).

The results of the antifungal activity obtained when *C. albicans* was exposed to zeolitic material and composites are presented in Fig. 4. The zeolitic materials Z-Na (Fig. 4a) and Z-NPsAgγ (Fig. 4b) have similar cellular decay behaviors as those for *S. typhimurium*, which means that Z-Na does not have an antifungal effect on *C. albicans* in contact with 200 and 2000 mg. However, the composite of silver achieves 100% mortality in 60 min, using a mass of 200 mg in both independent experiments (experiment 1 and experiment 2). For Z-NPsCuγ (Fig. 4c) and Z-NPsZnγ (Fig. 4d), were used 2000 mg of composite mass, but in both cases, no antifungal activity is observed. Again, Z-NPsAgγ has better efficiency as an antimicrobial against *C. albicans*, as well as it is for *S. thyphimurium,* although with 20 times more mass than the composite. Lara et al. (2015) reported that silver NPs have a positive charge, which causes damage to the cellular membrane and cell wall, making holes and pits, and allowing entry to small nanoparticles, which could induce apoptosis. On the other side, authors reported that zinc and copper oxides can exhibit effects against *C. albicans* (Karimiyan et al. 2015), due to the fact that they could generate oxidative stress. However, in the present work, the percent in weight of oxide-metallic NPs in the composites is low (around 1%), and probably, for this reason, the 100% mortality of yeast is not observed (Table 4).

Kinetic of the microbial mortality

Cell decay progress can be described mathematically by using Chick's model, which assumes that the concentration of composite is constant during the whole process and is characterized as a first-order kinetic (Ateia et al. 2020). Z-NPsAgγ composite shows the highest kinetic constant of decay for *S. typhimurium* with a mass of 10 mg, then Z-NPsCuγ, and finally Z-NPsZnγ, both using 200 mg. It can be observed in Table 3 that the ratio between the kinetic constants for two experiments is high for Z-NPsZnγ followed by Z-NPsCuγ, and finally Z-NPsAgγ. These results could be explained by the uniformity of the nanoparticles distributed on the zeolite network after the irradiation with the gamma rays from the ^{60}Co source. The nanoparticle sizes, the chemical speciation of them (ZnO, Cu_2O, and Ag^{o}), and their amount could also influence the antimicrobial activity of each composite.

In the case of *C. albicans*, Z-NPsAgγ has the highest kinetic constant (200 mg), followed by Z-NPsCuγ (2000 mg). It is important to note that there are differences

Table 4 Kinetic constants of cell decay of *C. albicans*

Sample	Metal content in the bulk of the composites	Mass of composite (mg)	Experiment number	Total inhibition time (min)	k (min^{-1})	R^2	k variation between experiments
ZNa	2.940 ± 0.150*	200	1	Not observed	NA	NA	NA
		2000	2	Not observed	NA	NA	NA
ZNPsAgγ	7.160 ± 0.001	200	1	60	0.0546	0.8476	k_{E2}/k_{E1} 1.8
			2	60	0.1003	0.9807	
ZNPsCuγ	1.910 ± 0.005	2000	1	Not was reached at 300	0.0041	0.8536	k_{E1}/k_{E2} 5.1
			2	Not was reached at 300	0.0008	0.7608	
			3	Not was reached at 420	0.0015	0.8436	k_{E1}/k_{E3} 2.7
							k_{E3}/k_{E2} 1.9
ZNPsZnγ	1.200 ± 0.004	2000	1	Not was reached at 300	0.0002	0.117	k_{E1}/k_{E2} 5.0
			2	Not was reached at 300	0.00004	0.048	

NA not applied

*Value determined by EDS

between the values of k (variation ratio between experiments) probably due to the distribution of NPs on the natural zeolite support, as was mentioned before; and the interaction that could establish the yeast with the copper composite (Table 4). The constant k was not able to be determined for Z-NPsZn based on the cellular decay behavior of the yeast. The results for Z-NPsAgγ agree with those observed by Rossainz-Castro et al. (2016), who report that silver composites have oligodynamic properties.

Composites in the disinfection process show a better effect on *S. typhimurium* than *C. albicans*, and it can be explained by factors such as *S. typhimurium*, as a Gram-negative bacteria, characterized by having a cell wall with lipid components, arranged in several layers (2–7 nm thin), besides an external cell membrane that allows the NPs to enter into the cells (Vanaja et al. 2013).

Demirci et al. (2014) reported that the composite of zeolite with Ag has an excellent antimicrobial effect, while those formed with Zn or Cu depend on the concentration since they are components of fungus and yeast. Composite Ag exhibited the most effectiveness against *S. typhimurium* and *C. albicans*, probably due to a major concentration of metal in the composite. Also, the silver ions can interact with sulfur groups such as di-sulfur and sulfhydryl (Dizaj et al. 2014), therefore damaging proteins. Du et al. (2017) have suggested two possible mechanisms to explain the antimicrobial action of metallic NPs. The first is about the adsorption of microorganisms on the composite's nanoparticles, and the second for the release of metallic ions from NPs supported on the composite to the aqueous media.

Conclusions

Three composites (nanoparticles of Ag, Cu_2O and ZnO supported on natural zeolite) are obtained using gamma irradiation with a total dose of 40 kGy and a dose rate of 0.756 kGy/h. Morphological analysis of these composites shows that the main component of zeolitic material is clinoptilolite and mordenite and that there is a small amount of quartz and feldspar. The crystallinity of the three composites is conserved after gamma-irradiation, while the Z-NPsAgγ has the highest metallic incorporation. The metallic or oxide-metallic NPs are supported by the zeolite, and all have a spherical shape with a size of less than 10 nm. The oxidation state of silver NPs are Ag(0); meanwhile, Cu has (I) and zinc (II) both in form of oxides. The surface area of the three composites has a slight increase in the comparison of material exchange with sodium. The silver composite reaches 100% of mortality at a minor time with less mass for both microorganisms (*S. typhimurium and C. albicans*) than the copper and zinc composites. The kinetic constant to the cellular decay for both microorganisms follows the order $k_{Z\text{-}NPsAg\gamma} > k_{Z\text{-}NPsCu\gamma} > k_{Z\text{-}NPsZn\gamma}$. Notably, differences between k values of two independent experiments exist for both microorganisms (bacteria and yeasts), using Z-NPsCuγ and Z-NPsZnγ composites. The kinetic constant of the cellular decay depends on the type of microorganism involved in the antimicrobial process (bacteria and yeast), as well as the characteristics of the composite obtained after the gamma irradiation using a ^{60}Co source. The Z-NpsAgγ composite is a good candidate to treat microbiologically contaminated water for potabilization purposes.

Conflicts of interest

The authors declare not to have conflicts of interest.

Supplementary Information The online version contains supplementary material available at https://doi.org/10.1007/s13204-021-01687-w.

Acknowledgments The authors are grateful for the financial assistance to project No. 254665 from the Mexican National Council for Science and Technology (CONACyT) and for the scholarship 553468; to ININ, for their support in instrumental analysis for the zeolitic material: TEM (I. Martínez), SEM and EDS (J. Pérez), XRD (P. López and L. Carapia), XPS (R. Basurto), BET (E. Morales) and neutron activation analysis NAA (J. Vidal), as well as irradiation of samples (D. Ortiz).

References

Abidin AZ, Abu-Bakar NHH, Ng EP, Tan WL (2017) Rapid degradation of methyl orange by Ag doped zeolite X in the presence of borohydride. J Taibah Univ Sci 11:1070–1079. https://doi.org/10.1016/j.jtusci.2017.06.004

Alswat AA, Bin AM, Saleh TA (2017) Preparation and characterization of zeolite/zinc oxide-copper oxide nanocomposite: antibacterial activities. Colloids Interface Sci Commun 16:19–24. https://doi.org/10.1016/j.colcom.2016.12.003

Alver BE, Sakizci M, Yörükoğullari E (2010) Investigation of clinoptilolite rich natural zeolites from Turkey: a combined XRF, TG/DTG, DTA and DSC study. J Therm Anal Calorim 100:19–26. https://doi.org/10.1007/s10973-009-0118-0

Ambrozova P, Kynicky J, Urubek T, Nguyen VD (2017) Synthesis and modification of clinoptilolite. Molecules 22:1–13. https://doi.org/10.3390/molecules22071107

Amini K, Kraatz HB (2014) Recent advances and developments in monitoring biological agents in water samples. Rev Environ Sci Biotechnol 14:23–48. https://doi.org/10.1007/s11157-014-9351-5

Ashbolt NJ (2015) Microbial contamination of drinking water and human health from community water systems. Curr Environ Heal Rep 2:95–106. https://doi.org/10.1007/s40572-014-0037-5

Ateia M, Alalm MG, Awfa D et al (2020) Modeling the degradation and disinfection of water pollutants by photocatalysts and composites: a critical review. Sci Total Environ 698:134197. https://doi.org/10.1016/j.scitotenv.2019.134197

Batistela VR, Fogaça LZ, Fávaro SL et al (2017) ZnO supported on zeolites: photocatalyst design, microporosity and properties. Colloids Surf A Physicochem Eng Asp 513:20–27. https://doi.org/10.1016/j.colsurfa.2016.11.023

Belloni J (2006) Nucleation, growth and properties of nanoclusters studied by radiation chemistry: application to catalysis. Catal Today 113:141–156. https://doi.org/10.1016/j.cattod.2005.11.082

Belloni J, Marignier JL, Mostafavi M (2018) Mechanisms of metal nanoparticles nucleation and growth studied by radiolysis. Radiat Phys Chem. https://doi.org/10.1016/j.radphyschem.2018.08.001

Bertrand JC, Caumette P, Lebaron P, et al (2015) Environmental microbiology: fundamentals and applications. Microb Ecol. https://doi.org/10.1007/978-94-017-9118-2

Biesinger MC (2017) Advanced analysis of copper X-ray photoelectron spectra. Surf Interface Anal 49:1325–1334. https://doi.org/10.1002/sia.6239

Bordbar M, Sharifi-Zarchi Z, Khodadadi B (2017) Green synthesis of copper oxide nanoparticles/clinoptilolite using *Rheum palmatum* L. root extract: high catalytic activity for reduction of 4-nitro phenol, rhodamine B, and methylene blue. J Sol-Gel Sci Technol 81:724–733. https://doi.org/10.1007/s10971-016-4239-1

Boruban C, Nalbant Esenturk E (2017) Synthesis of CuO nanostructures on zeolite-Y and investigation of their CO_2 adsorption properties. J Mater Res 32:3669–3678. https://doi.org/10.1557/jmr.2017.337

Bouzourâa MB, Naciri AE, Moadhen A et al (2016) Effects of silicon porosity on physical properties of ZnO films. Mater Chem Phys 175:233–240. https://doi.org/10.1016/j.matchemphys.2016.03.026

Cheon JY, Kim SJ, Rhee YH et al (2019) Shape-dependent antimicrobial activities of silver nanoparticles. Int J Nanomed 14:2773–2780. https://doi.org/10.2147/IJN.S196472

Clifford DC, Castano CE, Rojas JV (2017) Supported transition metal nanomaterials: nanocomposites synthesized by ionizing radiation. Radiat Phys Chem 132:52–64. https://doi.org/10.1016/j.radphyschem.2016.12.001

Copcia VE, Luchian C, Dunca S et al (2011) Antibacterial activity of silver-modified natural clinoptilolite. J Mater Sci 46:7121–7128. https://doi.org/10.1007/s10853-011-5635-0

De la Rosa-Gómez I, Olguín MT, Alcántara D (2008) Antibacterial behavior of silver-modified clinoptilolite-heulandite rich tuff on coliform microorganisms from wastewater in a column system. J Environ Manage 88:853–863. https://doi.org/10.1016/j.jenvman.2007.04.005

Demirci S, Ustaoğlu Z, Yilmazer GA et al (2014) Antimicrobial properties of zeolite-X and zeolite-A ion-exchanged with silver, copper, and zinc against a broad range of microorganisms. Appl Biochem Biotechnol 172:1652–1662. https://doi.org/10.1007/s12010-013-0647-7

Dizaj SM, Lotfipour F, Barzegar-Jalali M et al (2014) Antimicrobial activity of the metals and metal oxide nanoparticles. Mater Sci Eng C 44:278–284. https://doi.org/10.1016/j.msec.2014.08.031

Dong Y, Lin H, He Y (2017) Correlation between physicochemical properties of modified clinoptilolite and its performance in the removal of ammonia-nitrogen. Environ Monit Assess 189:1–10. https://doi.org/10.1007/s10661-017-5806-9

Du BD, Van PhuD, Quoc LA, Hien NQ (2017) Synthesis and investigation of antimicrobial activity of Cu_2O nanoparticles/zeolite. J Nanopart 2017:1–6. https://doi.org/10.1155/2017/7056864

Favvas EP, Tsanaktsidis CG, Sapalidis AA et al (2016) Clinoptilolite, a natural zeolite material: structural characterization and performance evaluation on its dehydration properties of hydrocarbon-based fuels. Microporous Mesoporous Mater 225:385–391. https://doi.org/10.1016/j.micromeso.2016.01.021

Feng L, Zhang C, Gao G, Cui D (2012) Facile synthesis of hollow Cu_2O octahedral and spherical nanocrystals and their morphology-dependent photocatalytic properties. Nanoscale Res Lett 7:1–10. https://doi.org/10.1186/1556-276X-7-276

Flores-Rojas GG, López-Saucedo F, Bucio E (2018) Gamma-irradiation applied in the synthesis of metallic and organic nanoparticles: a short review. Radiat Phys Chem 169:107962. https://doi.org/10.1016/j.radphyschem.2018.08.011

Ganguly P, Byrne C, Breen A, Pillai SC (2018) Antimicrobial activity of photocatalysts: fundamentals, mechanisms, kinetics and recent advances. Appl Catal B Environ 225:51–75. https://doi.org/10.1016/j.apcatb.2017.11.018

Hussain HM, Mohammed AAK (2019) Preparation and characterization of mordenite zeolite from Iraqi Sand. IOP Conf Ser Mater Sci Eng 518. https://doi.org/10.1088/1757-899X/518/6/062002

Jafari MJ, Zendehdel R, Rafieepour A et al (2020) Comparison of Y and ZSM-5 zeolite modified with magnetite nanoparticles in removal of hydrogen sulfide from air. Int J Environ Sci Technol 17:187–194. https://doi.org/10.1007/s13762-019-02348-w

Jiao W (2016) Facile synthesis of silver nanoparticles deposited on a calcium silicate hydrate composite as an efficient bactericidal agent. RSC Adv 6:112931–112938. https://doi.org/10.1039/c6ra24265k

Karimiyan A, Najafzadeh H, Ghorbanpour M, Hossein S (2015) Antifungal effect of magnesium oxide, zinc oxide, silicon oxide and copper oxide nanoparticles against *Candida albicans* Hekmati-Moghaddam. Zahedan J Res Med Sci 17:25–27. https://doi.org/10.17795/zjrms-2179

Khodadadi B, Bordbar M, Yeganeh-Faal A, Nasrollahzadeh M (2017) Green synthesis of Ag nanoparticles/clinoptilolite using Vaccinium macrocarpon fruit extract and its excellent catalytic activity for reduction of organic dyes. J Alloys Compd 719:82–88. https://doi.org/10.1016/j.jallcom.2017.05.135

Koopman JA, Marshall JM, Bhatiya A et al (2015) Inhibition of salmonella enterica biofilm formation using small- Molecule adenosine mimetics. Antimicrob Agents Chemother 59:76–84. https://doi.org/10.1128/AAC.03407-14

Korkuna O, Leboda R, Skubiszewska-Zieba J, Vrublevska T, Gunko VM, Ryczkowski J (2006) Structural and physicochemical properties of natural zeolites: clinoptilolite and mordenite. Microporous Mesoporous Mater 87:243–254. https://doi.org/10.1016/j.micromeso.2005.08.002

L'Annunziata MF (2007) Introduction: radioactivity and our well-being. Radioactivity 1–45. https://doi.org/10.1016/b978-044452715-8.50003-7

Lanje AS, Sharma SJ, Pode RB (2010) Synthesis of silver nanoparticles: a safer alternative to conventional antimicrobial and antibacterial agents. J Chem Pharm Res 2:478–483

Lara HH, Urbina DGR, Pierce C et al (2015) Effect of silver nanoparticles on *Candida albicans* biofilms : an ultrastructural study. J Nanobiotechnol 1–12. https://doi.org/10.1186/s12951-015-0147-8

León ER, Rodríguez EL, Beas CR et al (2016) Study of methylene blue degradation by gold nanoparticles synthesized within natural zeolites. J Nanomater 2016:9541683

Li Y, Yu J (2014) New stories of zeolite structures: their descriptions, determinations, predictions, and evaluations. Chem Rev 114:7268–7316. https://doi.org/10.1021/cr500010r

Li Y, Li L, Yu J (2017) Applications of zeolites in sustainable chemistry. Chem 3:928–949. https://doi.org/10.1016/j.chempr.2017.10.009

Lingaraju K, Raja Naika H, Manjunath K et al (2016) Biogenic synthesis of zinc oxide nanoparticles using *Ruta graveolens* (L.) and their antibacterial and antioxidant activities. Appl Nanosci 6:703–710. https://doi.org/10.1007/s13204-015-0487-6

Liu C, Zhang R, Wei S et al (2015) Selective removal of H_2S from biogas using a regenerable hybrid TiO_2/zeolite composite. Fuel 157:183–190. https://doi.org/10.1016/j.fuel.2015.05.003

Mahmoodi-Meimand M, Javid N, Malakootian M (2020) Adsorption of sulfur dioxide on clinoptilolite/nano iron oxide and natural adsorption of sulfur dioxide on clinoptilolite/nano iron oxide and natural clinoptilolite. Health Scope. https://doi.org/10.5812/jhealthscope.69158

Mansouri N, Rikhtegar N, Ahmad Panahi H et al (2013) Porosity, characterization and structural properties of natural zeolite—clinoptilolite—as a sorbent. Environ Prot Eng 39:139–152. https://doi.org/10.5277/EPE130111

Moradi M, Karimzadeh R, Moosavi ES (2018) Modified and ion exchanged clinoptilolite for the adsorptive removal of sulfur compounds in a model fuel: new adsorbents for desulfurization. Fuel 217:467–477. https://doi.org/10.1016/j.fuel.2017.12.095

Olorode OA, Okpokwasli GC (2012) The efficacy of disinfectants on abattoirs' *Candida albicans* isolates in Niger Delta region. F1000 Res 1:1–8. https://doi.org/10.12688/f1000research.1-20.v1

Panayotova MI, Mintcheva NN, Gemishev OT et al (2018) Preparation and antimicrobial properties of silver nanoparticles supported by natural zeolite clinoptilolite. Bulg Chem Commun 50:211–218

Pérez-González NK, Legorreta-García F, Díaz-Guzmán D, Vargas-Ramírez M, Reyes-Cruz VE, Flores-Zamora MI (2020) Determinación de las Características Físico-Químicas de una Zeolita Natural (Determination of physical-chemical characteristics of a natural zeolite). Pädi 8:14–18. https://doi.org/10.29057/icbi.v8iEspecial.6297

Polychroniadis EK, Oral AY, Ozer M (2013) International multidisciplinary microscopy congress. In: Proceedings of InterM, Antalya, Turkey. Springer

Rodríguez-Méndez BG, López-Callejas R, Olguín MT et al (2017) Growth of Ag particles from Ag-zeolite by pulsed discharges in water and their antibacterial activity. Microporous Mesoporous Mater 244:235–243. https://doi.org/10.1016/j.micromeso.2016.10.038

Rossainz-Castro LG, De-La-Rosa-Gómez I, Olguín MT, Alcántara-Díaz D (2016) Comparison between silver- and copper-modified zeolite-rich tuffs as microbicide agents for *Escherichia coli* and *Candida albicans*. J Environ Manage 183:763–770. https://doi.org/10.1016/j.jenvman.2016.09.034

Salama T, Ali IO (2016) Novel synthesis of nay zeolite from rice husk silica: modification with Zno and Zns for antibacterial application. Chem Sci J 07:1–9. https://doi.org/10.4172/2150-3494.1000118

Sareban Z, Javanbakht V (2017) Preparation and characterization of a novel nanocomposite of clinoptilolite/maghemite/chitosan/urea for manganese removal from aqueous solution. Korean J Chem Eng 34:2886–2900. https://doi.org/10.1007/s11814-017-0216-9

Sellam A, Whiteway M (2016) Recent advances on *Candida albicans* biology and virulence. F1000Res 5:2582. https://doi.org/10.12688/f1000research.9617.1

Shameli K, Bin AM, Yunus WMZW et al (2010) Synthesis of silver/montmorillonite nanocomposites using γ-irradiation. Int J Nanomed 5:1067–1077. https://doi.org/10.2147/IJN.S15033

Sharma P, Pant S, Poonia P et al (2018) Green synthesis of colloidal copper nanoparticles capped with *Tinospora cordifolia* and its application in catalytic degradation in textile dye: an ecologically sound approach. J Inorg Organomet Polym Mater 28:2463–2472. https://doi.org/10.1007/s10904-018-0933-5

Shaw R, Sharma R, Tiwari S, Tiwari SK (2016) Surface engineered zeolite: an active interface for rapid adsorption and degradation of toxic contaminants in water. ACS Appl Mater Interfaces 8:12520–12527. https://doi.org/10.1021/acsami.6b01754

Sheikh N, Akhavan A, Kassaee MZ (2009) Synthesis of antibacterial silver nanoparticles by γ-irradiation. Phys E Low Dimensional Syst Nanostruct 42:132–135. https://doi.org/10.1016/j.physe.2009.09.013

Shuai-Cheng W, Ben-Dong F, Xiu-Ling C et al (2016) Subinhibitory concentrations of phloretin repress the virulence of *Salmonella typhimurium* and protect against *Salmonella typhimurium* infection. Antonie van Leeuwenhoek Int J Gen Mol Microbiol 109:1503–1512. https://doi.org/10.1007/s10482-016-0752-z

Siddiqi KS, ur Rahman A, Tajuddin, Husen A (2018) Properties of zinc oxide nanoparticles and their activity against microbes. Nanoscale Res Lett 13. https://doi.org/10.1186/s11671-018-2532-3

Singh S, Bharti A, Meena VK (2015) Green synthesis of multi-shaped silver nanoparticles: optical, morphological and antibacterial properties. J Mater Sci Mater Electron 26:3638–3648. https://doi.org/10.1007/s10854-015-2881-y

Ullah R, Liu C, Panezai H et al (2019) Controlled crystal phase and particle size of loaded-TiO_2 using clinoptilolite as support via hydrothermal method for degradation of crystal violet dye in aqueous solution. Arab J Chem 13:4092–4101. https://doi.org/10.1016/j.arabjc.2019.06.011

Vanaja M, Gnanajobitha G, Paulkumar K et al (2013) Phytosynthesis of silver nanoparticles by *Cissus quadrangularis*: influence of physicochemical factors. J Nanostruct Chem 3:17. https://doi.org/10.1186/2193-8865-3-17

Vergara-Figueroa J, Alejandro-Martín S, Pesenti H, Cerda F, Fernández-Pérez A, Gacitúa W (2019) Obtaining nanoparticles of Chilean natural zeolite and its ion exchange with copper salt (Cu^{2+}) for antibacterial applications. Materials (Basel) 12:2202. https://doi.org/10.3390/ma12132202

Yu B, Wen Y, Yang X, Cai X (2019) Synthesis of ZnO–Au composite microspheres by one-pot polyol method and its application as a photo-catalyst. J Mater Sci Mater Electron 30:855–861. https://doi.org/10.1007/s10854-018-0356-7

Zahmakiran M, Durap F, Özkar S (2010) Zeolite confined copper(0) nanoclusters as cost-effective and reusable catalyst in hydrogen generation from the hydrolysis of ammonia-borane. Int J Hydrogen Energ 35:187–197. https://doi.org/10.1016/j.ijhydene.2009.10.055

Zahmakıran M, Akbayrak S, Salim C, Derya C (2011) Zeolite framework stabilized nickel (0) nanoparticles : active and long-lived catalyst for hydrogen generation from the hydrolysis of ammonia-borane and sodium borohydride. Catal Today 170:76–84. https://doi.org/10.1016/j.cattod.2010.09.022

Publisher's Note Springer Nature remains neutral with regard to jurisdictional claims in published maps and institutional affiliations.